Supporting Information for

Trapping & De-trapping in Colloidal Perovskite Nanoplatelets: Elucidation and Prevention of Nonradiative Processes through Chemical Treatment

Sander J.W. Vonk †, Magnus B. Fridriksson ‡, Stijn O.M. Hinterding †, Mark J.J. Mangnus †, Thomas P. van Swieten †, Ferdinand C. Grozema ‡, Freddy T. Rabouw † and Ward van der Stam †‡**

† Debye Institute, Utrecht University, Princetonplein 1,The Netherlands

‡ Opto-Electronic Materials Section, Faculty of Applied Sciences, Delft University of Technology, van der Maasweg 9, 2629 HZ Delft, The Netherlands

* Corresponding authors. E-mail: w.vanderstam@uu.nl and f.t.rabouw@uu.nl

Methods

Materials: Lead bromide ($PbBr_2$, 99.999%), cesium carbonate (Cs_2CO_3, 99%), oleic acid (OA, >99%), oleylamine (technical grade, 70%), anhydrous hexane, acetone and toluene were purchased from Sigma-Aldrich and used as received.

Precursor solution preparation: A Cs-oleate precursor solution was prepared by dissolving Cs_2CO_3 (0.1 mmol) in oleic acid (10 mL) at 100 °C.[S1] A $PbBr_2$ treatment precursor solution was prepared by dissolving $PbBr_2$ (0.1 mmol) in a mixture of oleic acid (0.1 mL), oleylamine (0.1 mL) and hexane (10 mL) at 100 °C. A $PbBr_2$ synthesis precursor was prepared by dissolving $PbBr_2$ (0.1 mmol) in a mixture of oleic acid (0.1 mL), oleylamine (0.1 mL) and toluene (10 mL) at 100 °C. All mixtures were vigorously stirred and heated in order to dissolve the salts, after which transparent, colorless precursor solutions were obtained.

Synthesis and treatment of $CsPbBr_3$ nanoplatelets: The $CsPbBr_3$ nanoplatelets (NPLs) were all synthesized following the protocol of Bohn et al.[S2] In brief, for the synthesis of 4 monolayer (ML) $CsPbBr_3$ NPLs, 150 μL Cs-oleate precursor was injected into 1.2 mL $PbBr_2$ synthesis precursor, while continuously stirring the reaction solution. After ∼5 s, 2 mL acetone was swiftly added in order to initiate the crystallization of the NPLs. After 1 min, the stirring was terminated and the solution was centrifuged (3500 rpm, 5 min) in order to separate the NPLs from unreacted precursor. For the synthesis of 6 ML NPLs, all synthesis steps are the same as described above, except for the amounts of (precursor) solution (250 μL Cs-oleate precursor, 1 mL $PbBr_2$ synthesis precursor with 0.3 mL acetone added, and 2.5 mL acetone). All syntheses were conducted under ambient conditions. To treat the NPLs, 0.1 mL of the $PbBr_2$ treatment precursor solution was added to diluted (10^{-8} M) NPL dispersions under vigorous stirring.

Steady-state optical spectroscopy: The absorbance of $CsPbBr_3$ NPL solutions was measured on a Perkin Elmer Lambda 900 UV/VIS/NIR Spectrometer. The steady-state photoluminescence (PL) was measured on an Edinburgh Instruments FLS980 Fluorescence Spectrometer, using a 450 W Xenon lamp as the excitation source (excitation wavelength 405 nm). PLQY measurements were carried out in the same device, using an integrating sphere. Solutions were measured in closed quartz cuvettes (pathlength 10 mm). Diluted solutions were prepared by adding 50–100 μL of the crude NPLs in hexane solution (concentration 10^{-8} M) to 3 mL hexane in quartz cuvettes, in order to reach an optical density at the excitation wavelength of 405 nm around 0.1.[S3, S4]

Transmission electron microscopy and x-ray diffraction: Transmission electron microscopy samples were prepared by drop-casting a dilute solution of NPLs in hexane on a carbon-coated copper TEM grid (400-mesh). TEM images and electron diffraction patterns were measured on a JEOL JEM-1400 TEM, operating at 120 kV. X-ray diffraction samples were prepared by drying a concentrated solution of NPLs,

the dry powder was put on a silicon wafer. X-ray diffraction patterns were measured using a Bruker D2 Phaser using a Co X-ray source ($\lambda = 1.79$ Å).

Streak camera measurements: The time-resolved photoluminescence streak camera measurements were performed using a Hamamatsu C5680 streak camera setup. The samples were excited with a Chameleon Ultra II (Ti:Sapph) oscillator combined with a harmonic generator producing 140 fs pulses with a repetition rate of 80 MHz at a fluence of $\sim$1 μJ cm^{-2} corresponding to an average number of excitons per pulse of $\langle N \rangle \approx 0.03$–$0.04$. This range is obtained by assuming an intrinsic absorption coefficient of $CsPbBr_3$ at 400 nm in hexane of 7.7×10^4 cm^{-1}, lateral dimensions of 8 nm $\times$ 8 nm and a NPL thickness of 2.4 nm (4ML) and 3.4 nm (6ML) giving absorption cross sections of 1.2×10^{-14} cm^2 (4ML) and 1.7×10^{-14} cm^2 (6ML).[S4] The NPL dispersion was stirred during the measurement to minimize sedimentation and beam damage by the laser. An excitation wavelength of 405 nm was used in order to match the settings of the TCSPC pulsed laser. The time ranges of the streak camera measurements were 0.13 ns for the high-resolution measurement and 1.22 ns for the low-resolution measurement. The time resolution of the setup is 3 ps.

TCSPC measurements: Nanosecond time-correlated single-photon counting (TCSPC) measurements were performed on an Edinburg Instrument FLS920 fluorescence spectrometer, using a PicoQuant pulsed diode laser (wavelength 405 nm) with a repetition rate of 0.5 MHz at a fluence of $\sim$0.1 nJ cm^{-2}. The NPL dispersion was stirred during the measurement to minimize sedimentation and beam damage by the laser. Emission events were time-correlated with the excitation pulses using an Edinburgh TCC900 computer card.

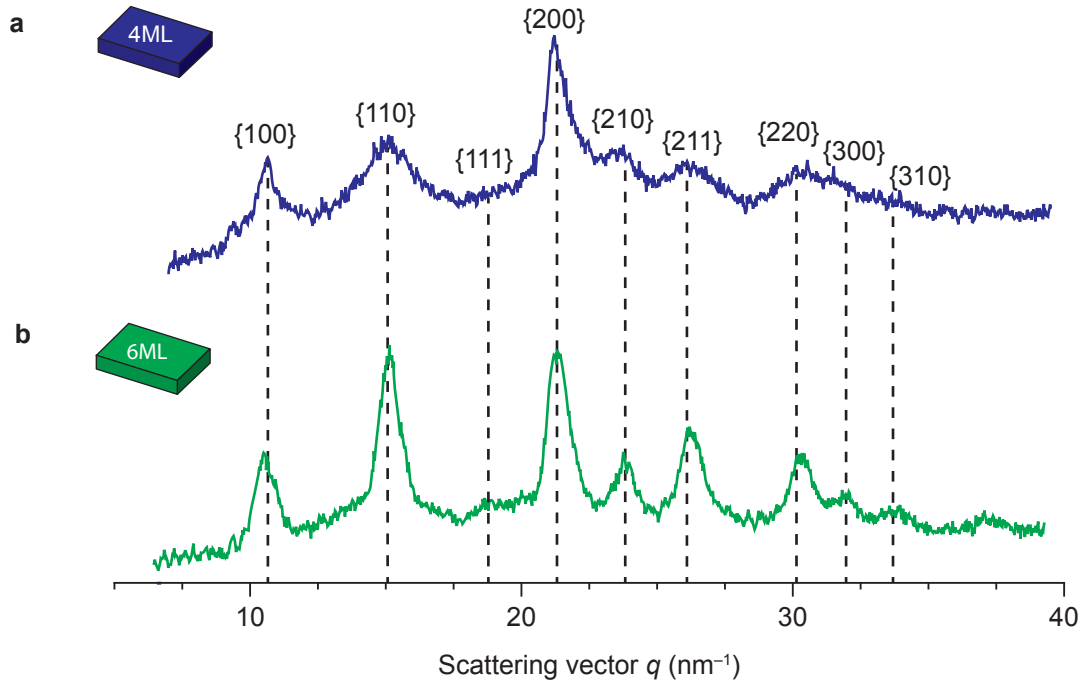

Figure S1 | X-ray diffraction of $CsPbBr_3$ nanoplatelets. X-ray diffraction pattern of **(a)** 4ML and **(b)** 6ML NPLs. The dashed lines show the characteristic lattice planes of a cubic perovskite crystal structure with a lattice constant $a = 5.897$ Å.[S6]

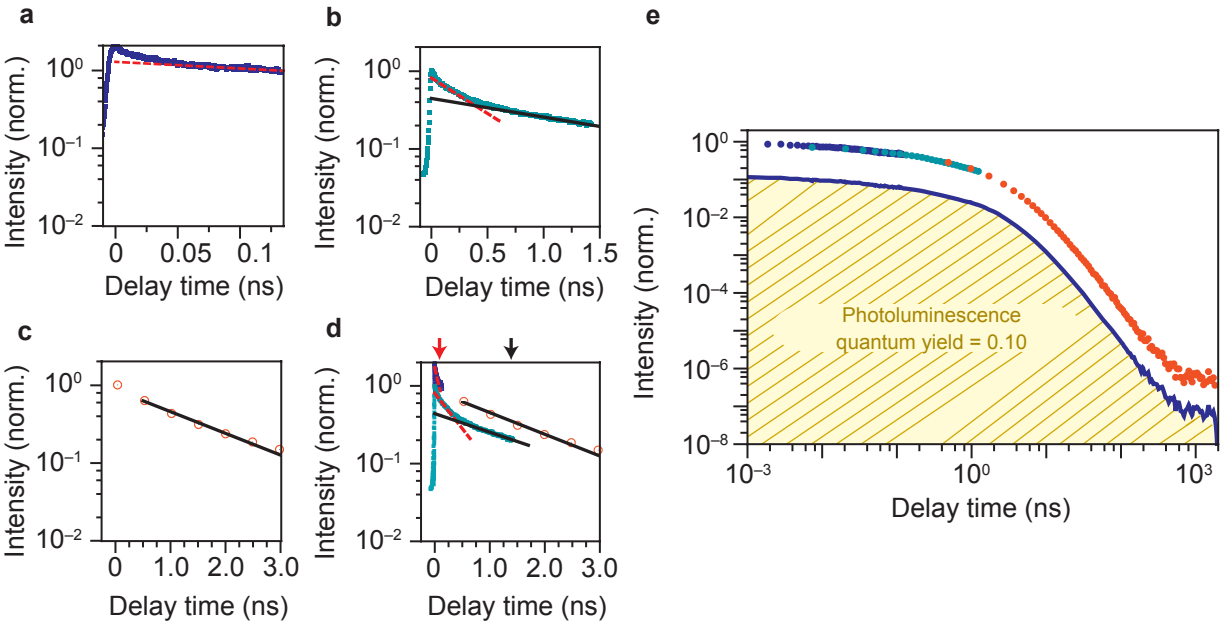

Figure S2 | Stitching of streak camera and TCSPC measurements. **(a)** The high-resolution streak camera measurement was fitted to a single-exponential function $A(t)$ (red, dashed) for delay times $t > 75$ ps. **(b)** The low-resolution streak camera measurement was fitted to a single-exponential function on the domain 0.1 ns $< t <$ 0.18 ns (red, dashed) and to a second single-exponential function $C(t)$ on the domain $t > 0.7$ ns (black). **(c)** The TCSPC measurement was fitted to a single-exponential function $D(t)$ on the domain 0.5 ns $< t <$ 3 ns. **(d)** We stitch the three measurements together by adjusting the relative intensity scales such that $A(133\text{ ps}) = B(133\text{ ps})$ (red arrow) and $C(1.43\text{ ns}) = D(1.43\text{ ns})$ (black arrow). **(e)** The stitching procedure yields the total decay curve ranging from the ps timescale of the streak camera to the μs timescale of the TCSPC measurement. To obtain the quantum yield density $\phi(t)$ we normalized the total area under the decay curve to the PLQY of the nanoplatelet samples.

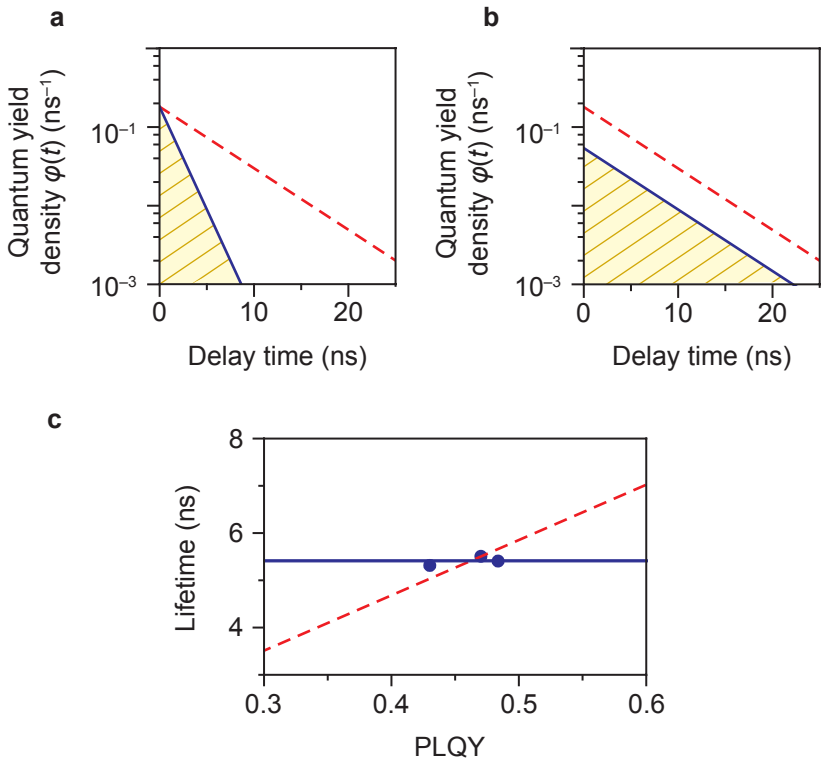

Figure S3 | The dark fraction and determination of the radiative rate. Here, we consider two scenarios in which a sample of emitters, e.g. perovskite nanoplatelets, have non-unity PLQY but a quantum yield density $\phi(t)$ that is qualitatively different. **(a)** The first scenario we consider is a sample in which all emitters are identical. The quantum yield density is given by

$$\phi(t) = k_{\mathrm{rad}} \mathrm{e}^{-(k_{\mathrm{rad}}+k_{\mathrm{nr}}^{\mathrm{B}})t},$$

where the amplitude $\phi(0)$ is equal to the radiative rate k_{rad}, the nonradiative rate of the bright fraction is $k_{\mathrm{nr}}^{\mathrm{B}}$ and the PLQY is equal to $k_{\mathrm{rad}}/(k_{\mathrm{rad}} + k_{\mathrm{nr}}^{\mathrm{B}})$. The red dashed line shows the quantum yield density for a unity PLQY sample based on a radiative rate $k_{\mathrm{rad}} = 0.18$ ns^{-1} and $k_{\mathrm{nr}}^{\mathrm{B}} = 0$ ns^{-1}. A decrease of the PLQY (blue, $k_{\mathrm{nr}}^{\mathrm{B}} = 0.42$ ns^{-1} and PLQY $= 0.3$) in this scenario will make the excited-state dynamics faster but the amplitude is unchanged. **(b)** The second scenario is a sample in which we have two subpopulations, one with unity PLQY ($k_{\mathrm{nr}}^{\mathrm{B}} = 0$ ns^{-1}) called the bright fraction and one with zero PLQY called the dark fraction. We can write the quantum yield density as

$$\phi(t) = f k_{\mathrm{rad}} \mathrm{e}^{-k_{\mathrm{rad}}t} + (1-f) k_{\mathrm{rad}} \mathrm{e}^{-(k_{\mathrm{rad}}+k_{\mathrm{nr}}^{\mathrm{D}})t},$$

where f is the bright fraction and the PLQY equals the bright fraction f. The excited-state dynamics of the dark fraction are completely masked by the instrument response function (IRF) of the TCSPC and streak camera measurements because $k_{\mathrm{nr}}^{\mathrm{D}} \gg k_{\mathrm{rad}}, \tau_{\mathrm{IRF}}^{-1}$ which effectively lowers the amplitude of the quantum yield density to $\phi(0) = f k_{\mathrm{rad}}$. The red dashed line shows the quantum yield density of a unity-PLQY sample based on a radiative rate $k_{\mathrm{rad}} = 0.18$ ns^{-1} and $f = 1$. Here, a decrease of the PLQY (blue, $f = 0.3$) corresponds to an increase of the dark fraction which lowers the amplitude of the quantum yield density. **(c)** To verify which of the scenarios describe our nanoplatelet samples we measured the lifetimes for three independently synthesized 4-monolayer nanoplatelet samples. The samples are nominally the same but differ slightly in PLQY. Based on the assumption that we have a dark fraction of nanoplatelets we expect that the measured lifetime $\tau = 1/k_{\mathrm{rad}}$ is constant (blue) for the three samples and the PLQY is different only because of sample-to-sample variations of the bright fraction f. If we assumed one population of imperfect nanoplatelets, the PLQY $= k_{\mathrm{rad}}\tau$ would scale linearly (red, dashed) with the radiative rate. We observe that the lifetime is constant with different PLQY and therefore we assign the non-unity PLQY to the presence of a dark fraction which lowers the PLQY and identify the fitted decay rate $k_{\mathrm{rad}} = 0.18$ ns^{-1} as the radiative decay rate.

Delayed emission mechanisms with varying nonradiative rates

Temporary storage and release of excitonic charge carriers can result in photon emission with a relatively long delay time compared to direct radiative emission. From the quantum yield density $\phi(t)$ we observe slower and faster dynamics with respect to radiative recombination. These observations can be explained by two qualitatively different delayed-emission mechanisms. The first scenario is [1] hot-carrier trapping where one of the charge carriers is trapped from a hot-exciton state. The second mechanism is [2] cold-carrier trapping where the exciton cools down to the lowest-energy exciton state before a charge carrier is trapped. Here, we will discuss the influence of a chemical treatment—which changes the nonradiative processes—on the fraction of delayed emission to reveal the predominant delayed-emission mechanism in perovskite nanoplatelets. We will assume that radiative recombination from a stored charge carrier does not occur in our samples, because no trap-state emission is observed in the emission spectra (Figure 2c–d).

[1] In the scenario of hot-carrier trapping (Figure S3a) the trapping rate $k_{\mathrm{trap}}^{\mathrm{hot}}$ is in competition with hot-exciton cooling k_{c}. The probability that an absorption event leads to delayed emission

$$\eta_{\mathrm{delayed}}^{\mathrm{hot}} = \frac{f k_{\mathrm{rad}}}{k_{\mathrm{rad}} + k_{\mathrm{nr}}} \frac{k_{\mathrm{trap}}^{\mathrm{hot}}}{k_{\mathrm{trap}}^{\mathrm{hot}} + k_{\mathrm{c}}}, \tag{1}$$

is the product of the probability for hot-carrier trapping and the probability for photon emission after release. Because cooling rates are typically very fast 0.3 ps^{-1}, in this case $k_{\mathrm{trap}}^{\mathrm{hot}}$ must be similarly fast in order to compete with cooling.[S5] The probability that an absorption event leads to prompt emission

$$\eta_{\mathrm{prompt}}^{\mathrm{hot}} = \frac{f k_{\mathrm{rad}}}{k_{\mathrm{rad}} + k_{\mathrm{nr}}} \frac{k_{\mathrm{c}}}{k_{\mathrm{hot,trap}} + k_{\mathrm{c}}}, \tag{2}$$

is the product of the probability for hot-exciton cooling and the probability for photon emission after cooling. From the two expressions above we observe that lowering of the nonradiative recombination rate k_{nr} increases both $\eta_{\mathrm{prompt}}^{\mathrm{hot}}$ and $\eta_{\mathrm{delayed}}^{\mathrm{hot}}$. However, both decay pathways to the ground state experience the nonradiative quenching only once. Therefore the contribution of delayed photons to the total emission

$$x_{\mathrm{delayed}}^{\mathrm{hot}} = \frac{\eta_{\mathrm{delayed}}^{\mathrm{hot}}}{\eta_{\mathrm{prompt}}^{\mathrm{hot}} + \eta_{\mathrm{delayed}}^{\mathrm{hot}}} = \frac{k_{\mathrm{trap}}^{\mathrm{hot}}}{k_{\mathrm{trap}}^{\mathrm{hot}} + k_{\mathrm{c}}}, \tag{3}$$

is independent of k_{nr}. Figure S3b shows the contribution of delayed photons to the total emission before (PLQY = 0.10) and after (PLQY = 0.44) treatment with $PbBr_2$. The constant contribution of delayed photons to the total emission for hot-carrier trapping (red, dashed) does not match the measurements and therefore we exclude hot-carrier trapping as the dominant mechanism underlying delayed emission.

[2] In the scenario of cold-carrier trapping (FigureS3c and e) the trapping rate $k_{\mathrm{cold,\ trap}}$ is in competition with radiative and nonradiative recombination. The probability that an absorption event leads to prompt emission is

$$\eta_{\mathrm{prompt}}^{\mathrm{cold}} = \frac{f k_{\mathrm{rad}}}{k_{\mathrm{rad}} + k_{\mathrm{nr}} + k_{\mathrm{trap}}^{\mathrm{cold}}}, \tag{4}$$

where $k_{\mathrm{trap}}^{\mathrm{cold}}$ is the trapping rate of cold charge carriers. Similarly, we can define the contribution of delayed emission to the total decay. In this scenario charge carriers can cycle an arbitrary number of times between the trap state and the lowest-energy exciton state. To obtain the total probability for delayed emission we sum over all possible cycles $n \geq 1$ and multiply with the probability that a photon is emitted from the lowest-energy exciton state:

$$\eta_{\mathrm{delayed}}^{\mathrm{cold}} = \frac{f k_{\mathrm{rad}}}{k_{\mathrm{rad}} + k_{\mathrm{nr}} + k_{\mathrm{trap}}^{\mathrm{cold}}} \sum_{n=1}^{\infty} \left(\frac{k_{\mathrm{trap}}^{\mathrm{cold}}}{k_{\mathrm{rad}} + k_{\mathrm{nr}} + k_{\mathrm{trap}}^{\mathrm{cold}}} \right)^{n}. \tag{5}$$

The infinite sum is a geometric series which we can simplify writing $\eta^{\text{cold}}_{\text{delayed}}$ in terms of all the rates as

$$\eta^{\text{cold}}_{\text{delayed}} = \frac{f k_{\text{rad}} k^{\text{cold}}_{\text{trap}}}{(k_{\text{rad}} + k_{\text{nr}} + k^{\text{cold}}_{\text{trap}})(k_{\text{rad}} + k_{\text{nr}})}. \tag{6}$$

Using the expressions of the prompt- and delayed-emission probabilities derived above gives the fraction of delayed emission

$$x^{\text{cold}}_{\text{delayed}} = \frac{\eta^{\text{cold}}_{\text{delayed}}}{\eta^{\text{cold}}_{\text{prompt}} + \eta^{\text{cold}}_{\text{delayed}}} = \frac{k^{\text{cold}}_{\text{trap}}}{k_{\text{rad}} + k_{\text{nr}} + k^{\text{cold}}_{\text{trap}}}. \tag{7}$$

We see that a large trapping rate $k^{\text{cold}}_{\text{trap}}$ compared to radiative- and nonradiative recombination rates leads to a high fraction of delayed emission. Next, we distinguish between two possibilities of how the treatment affects the nonradiative rates. In the first possibility (Figure S3c), we assume that the treatment only affects the nonradiative recombination rate k_{nr}. In the second possibility (Figure S3e), we assume that both nonradiative recombination and the trapping rate are affected by the treatment.

[2A] In the first possibility where only nonradiative recombination is affected by the treatment (Figure S3c), we can use the relationship between the nonradiative recombination rate and the PLQY

$$\text{PLQY} = \frac{f k_{\text{rad}}}{k_{\text{rad}} + k_{\text{nr}}} \tag{8}$$

to express the contribution of delayed photons to the total emission $x^{\text{cold}}_{\text{delayed}}$ in terms of the PLQY:

$$x^{\text{cold}}_{\text{delayed}} = \frac{1}{1 + \frac{f k_{\text{rad}}}{\text{PLQY} k^{\text{cold}}_{\text{trap}}}}. \tag{9}$$

In Figure S3d we compare equation S9 to the experimental relation between PLQY and $x^{\text{cold}}_{\text{delayed}}$. For a fitted trapping rate of $k^{\text{cold}}_{\text{trap}} = 5.6\ \mu\text{s}^{-1}$ we observe an increase of the contribution of delayed photons to the total emission. Therefore we exclude this scenario to contribute to delayed emission.

[2B] In the second possibility for cold-carrier trapping, we assume that both the trapping rate $k^{\text{cold}}_{\text{trap}}$ and the nonradiative recombination rate k_{nr} change to the same extent, *i.e.* by the same factor (Figure S3e). The contribution of delayed emission to the total emission is given by

$$x^{\text{cold}}_{\text{delayed}} = \frac{1}{1 + \frac{f}{a(f - \text{PLQY})}}, \tag{10}$$

where a is the ratio between the trapping rate $k^{\text{cold}}_{\text{trap}}$ and the nonradiative recombination rate k_{nr}.
In Figure S2f we compare equation S10 to the experimental relation between PLQY and $x^{\text{cold}}_{\text{delayed}}$. For a fitted constant ratio $a = 0.039$ we observe a decrease of the delayed emission fraction as a function of the PLQY consistent with the experiments. We therefore conclude that cold-carrier trapping is the dominant trapping- and release mechanism for excitons in 4- and 6-monolayer perovskite nanoplatelets and that both trap states leading to nonradiative recombination and delayed emission are supressed by the chemical treatment.

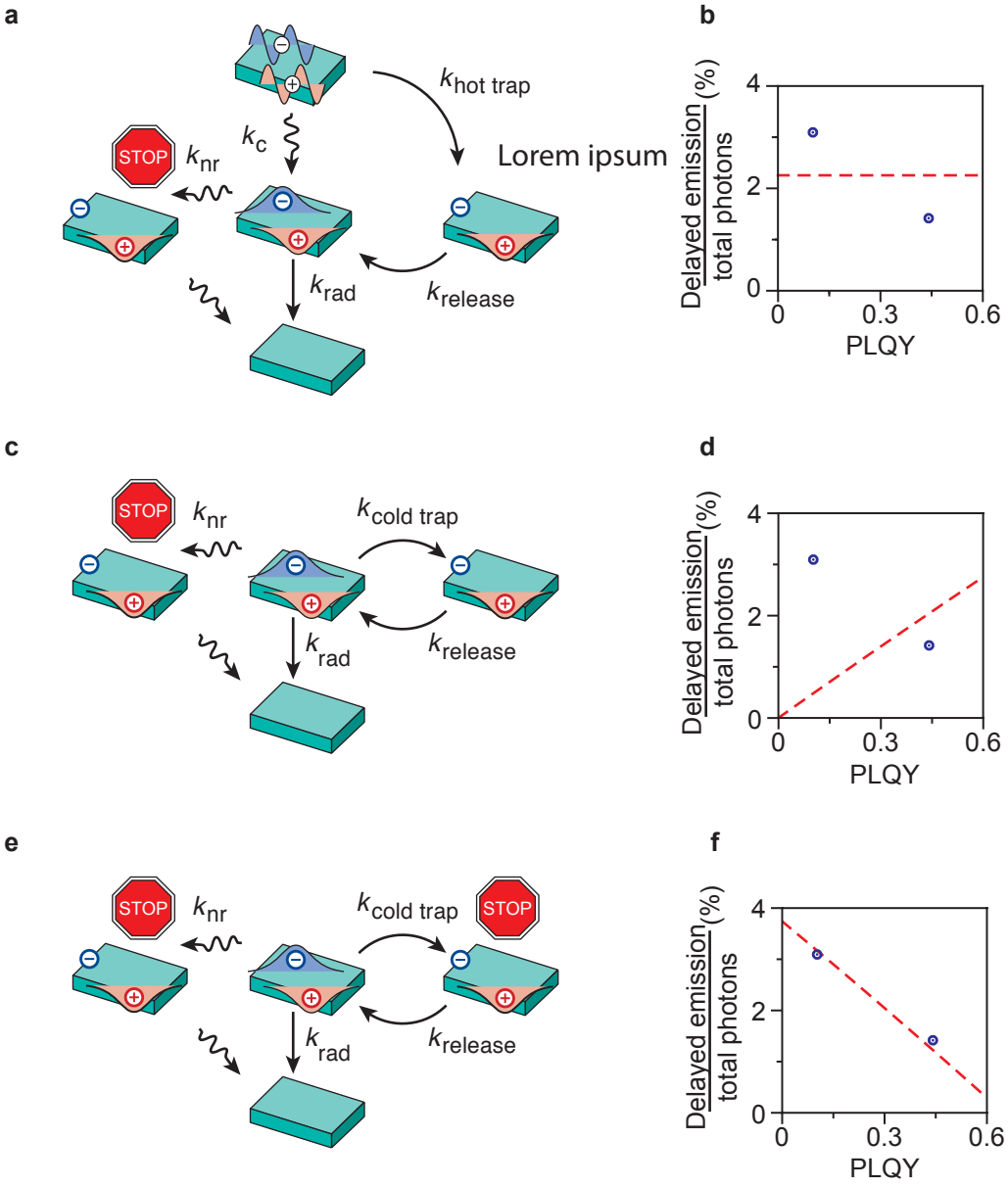

Figure S4 | Mechanisms for delayed exciton recombination. **(a)** Scenario [1], in which hot-carrier trapping from a hot-exciton state leads to delayed emission of photons. The treatment suppresses nonradiative recombination from band-edge excitons. **(b)** Fraction of delayed emission $x^{\mathrm{hot}}_{\mathrm{delayed}}$ for 4-monolayer perovskite nanoplatelet sample before (PLQY = 0.10) and after (PLQY = 0.44) treatment with $PbBr_2$. Assuming a constant trapping rate $k_{\mathrm{hot,trap}}$ and varying nonradiative recombination rate k_{nr} (equation S3) yields a constant delayed emission fraction as a function of the PLQY. **(c)** Scenario [2A], in which cold-carrier trapping from a band-edge exciton leads to delayed emission of photons. The treatment suppresses nonradiative recombination from band-edge excitons. **(d)** Same as b, but now plotting the calculated $x^{\mathrm{cold}}_{\mathrm{delayed}}$ in scenario [2A] (equation S9, $k^{\mathrm{cold}}_{\mathrm{trap}} = 5.6\ \mu\mathrm{s}^{-1}$). **(e)** Scenario [2B], in which cold-carrier trapping from a band-edge exciton leads to delayed emission of photons. The treatment suppresses both nonradiative recombination from band-edge excitons as well as nonradiative temporary trapping. **(f)** Same as b, but now plotting the calculated $x^{\mathrm{cold}}_{\mathrm{delayed}}$ in scenario [2B] (equation S10, $a = 0.039$)

Timescale between trapping and emission

To determine the timescale between trapping and emission of a delayed photon we have to solve the rate equations for the population of the excited state $N_{\mathrm{E}}(t)$ and the trap state $N_{\mathrm{T}}(t)$:

$$\dot{N}_{\mathrm{E}}(t) = -(k_{\mathrm{rad}} + k_{\mathrm{trap}})N_{\mathrm{E}}(t) + k_{\mathrm{rel}}N_{\mathrm{T}}(t) \tag{11a}$$

$$\dot{N}_{\mathrm{T}}(t) = -k_{\mathrm{rel}}N_{\mathrm{T}}(t) + k_{\mathrm{trap}}N_{\mathrm{E}}(t). \tag{11b}$$

Here the excited-state population $N_{\mathrm{E}}(t)$ decreases in time due to radiative recombination k_{rad} and trapping k_{trap} and the population increases by release of charge carriers k_{rel} by the trap state. The trap-state population $N_{\mathrm{T}}(t)$ decreases in time by release of charge carriers k_{rel} and increases by trapping k_{trap}. We can calculate expressions for both populations in time assuming that all initial population is in the trap state ($N_{\mathrm{E}}(0) = 0$ and $N_{\mathrm{T}}(0) = 1$). We obtain the population dynamics of the exciton state

$$N_{\mathrm{E}}(t) = \frac{2k_{\mathrm{rel}}\mathrm{e}^{-Kt/2}\sinh(\sqrt{K^2 - 4k_{\mathrm{rad}}k_{\mathrm{rel}}}t/2)}{\sqrt{K^2 - 4k_{\mathrm{rad}}k_{\mathrm{rel}}}}, \tag{12}$$

where $K = k_{\mathrm{rad}} + k_{\mathrm{trap}} + k_{\mathrm{rel}}$. We can use these dynamics to calculate the average time $\langle\tau\rangle$ for a charge carrier to de-trapped

$$\langle\tau\rangle = \frac{\int_0^\infty tN_{\mathrm{E}}(t)\mathrm{d}t}{\int_0^\infty N_{\mathrm{E}}(t)\mathrm{d}t} = k_{\mathrm{rad}}^{-1} + k_{\mathrm{rel}}^{-1} + \frac{k_{\mathrm{trap}}}{k_{\mathrm{rad}}k_{\mathrm{rel}}}, \tag{13}$$

where the average time between trapping and emission is equal to $\langle\tau\rangle = k_{\mathrm{rad}}^{-1} + k_{\mathrm{rel}}^{-1}$ when we assume that a charge carrier is only trapped once, or $k_{\mathrm{trap}} \ll k_{\mathrm{rad}}, k_{\mathrm{rel}}$.

Supporting References

(S1) Wang, Y.; Zhi, M.; Chang, Y. Q.; Zhang, J.; Chan, Y. Stable , Ultralow Threshold Amplified Spontaneous Emission from $CsPbBr_3$ Nanoparticles Exhibiting Trion Gain, *Nano Lett.* **2018**, *18*, 4976–4984.

(S2) Bohn, B. J.; Tong, Y.; Gramlich, M.; Lai, M. L.; Döblinger, M.; Wang, K.; Hoye, R. L. Z.; Muller-Buschbaum, P.; Stranks, S. D.; Urban, A. S. Boosting Tunable Blue Luminescence of Halide Perovskite Nanoplatelets through Post-Synthetic Surface Trap Repair, *Nano Letters* **2018**, *18*, 5231–5238.

(S3) de Roo, J.; Ibáñez, M.; Geiregat, P.; Nedelcu, G.; Walravens, W.; Maes, J.; Martins, J. C.; Van Driessche, I.; Kovalenko, M. V.; Hens, Z. Highly Dynamic Ligand Binding and Light Absorption Coefficient of Cesium Lead Bromide Perovskite Nanocrystals, *ACS Nano* **2016**, *10*, 2071–2081.

(S4) Maes, J.; Balcaen, L.; Drijvers, E.; Zhao, Q.; de Roo, J.; Vantomme, A.; Vanhaecke, F.; Geiregat, P.; Hens, Z. Light Absorption Coefficient of $CsPbBr_3$ Perovskite Nanocrystals, *J. Phys. Chem. Lett.* **2018**, *9*, 3093–3097.

(S5) Chen, J.; Messing, M.; Zheng, K.; Pullerits, T. Cation-Dependent Hot Carrier Cooling in Halide Perovskite Nanocrystals, *J. Am. Chem. Soc.* **2019**, *141*, 3532–3540.

(S6) van der Stam, W.; Geuchies, J.J.; Altantzis, T.; van den Bosch, K.H.W; Meeldijk, J.D.; van Aert, S.; Bals, S.; Vanmaekelbergh, D.; de Mello Donega, C. Highly Emissive Divalent-Ion-Doped Colloidal $CsPb_{1-x}M_xBr_3$ Perovskite Nanocrystals through Cation Exchange Nanocrystals, *J. Am. Chem. Soc.* **2017**, *139*, 4087–4097.